DOI: 10.61782/fa.2023.0393

forum acusticum 2023

MEMS LOUDSPEAKER FOR IN-EAR APPLICATION

Romain Liechti[1*] **Stéphane Durand**[2] **Thierry Hilt**[1]
Fabrice Casset[1] **Mikaël Colin**[1]
[1] CEA-Leti, Univ. Grenoble Alpes, F-38000 Grenoble, France
[2] LAUM, Le Mans Université, F-72085 Le Mans, France

ABSTRACT

A growing interest for MEMS loudspeakers for in-ear applications has been observed in recent years, with encouraging results in terms of sound pressure level, distortion and form factor [1–3]. MEMS loudspeakers based on thin film PZT are promising to replace advantageously the bulky loudspeakers that are currently used in small wearable devices. Reducing the size of loudspeakers and adapt them to micro-fabrication processes could allow to reduce further the power consumption and to integrate them in smaller devices, such as smart-watches and true wireless earbuds. In this paper we present the measurement results of the loudspeaker presented in [4] and the comparison of the results with the simulation carried with a lumped element model and a finite element model presented in [5]. In the simulations performed with both lumped parameters and finite elements models, the loudspeaker produces a sound pressure level of more than $120\,\mathrm{dB_{SPL}}$ down to $100\,\mathrm{Hz}$. The response of the loudspeaker is measured using a G.R.A.S RA0045 ear-occluded coupler, following the International 60318-4 (IEC) standard. The back cavity of the loudspeaker is unloaded and the setup is placed inside an anechoic G.R.A.S chamber. An adapter is designed and 3D printed in order to adapt the moving plate of the loudspeaker to the input of the ear-occluded coupler. The Total Harmonic Distortion (THD), due to the complex non-linear behaviour of the thin film piezoelectric material used in the loudspeaker, is evaluated as well. The differences observed between the experimental results and the models are then explained, and ways of improving the models and the performance of the loudspeaker are discussed.

Keywords: *In-Ear, MEMS, Piezoelectric, Loudspeaker*

**Corresponding author*: *romain.liechti@cea.fr.*

1. INTRODUCTION

The constant increase of the number of publications about research on MEMS loudspeakers could be attributed to the growing interest of the industry for this technology, stimulated by the recent significant improvement of the performance. Although loudspeakers dedicated to free field application are still not able to reach the acoustic pressure generated at low frequencies by larger non-MEMS micro loudspeakers, recent publications have shown interesting performance for in-ear applications [6–8]. For in-ear applications, MEMS loudspeaker are offering significant advantages, such as low manufacturing tolerances, ideal for active noise cancellation and channel matching as well as low power consumption. Despite reaching sound pressure level as high as $115\,\mathrm{dB_{SPL}}$ at $20\,\mathrm{Hz}$, these loudspeaker are suffering from the high (several tens of per cent) Total Harmonic Distortion (THD) originating from the non-linear character of their transduction either based on electrostatic or piezoelectric effects. To reduce the THD generated by these loudspeakers down to an inaudible limit, complex non-linear models as well as non-linear real time signal processing can be used but are significantly increasing the price and the power consumption of the system. A simpler way to decrease the THD would be to increase the sensitivity of the loudspeaker, in order to reach similar sound pressure levels for lower input voltages. To obtain a high sensitivity, our loudspeaker is based on a innovative manufacturing process, in which the electro-mechanical transduction of the loudspeaker, composed of piezoelec-

tric bending actuators is separated from the mechano-acoustical transduction performed by a rigid moving plate. On the other hand, accurate modelling of loudspeakers is essential to tune the acoustic response of the driver when designing the enclosure in order to reach the target frequency response [9]. To evaluated the performance of the loudspeaker inside the coupler, a lumped element model as well as two-port models to represent ducts in the plane wave assumption are used and are giving good agreements with the measured data. With a dedicated packaging, the pressure reached by our loudspeaker could be increased by 10 dB by reducing the volume between the radiating surface and the microphone of the coupler. To reach a higher sound pressure level in low frequencies, a correct sealing should be obtained between the loudspeaker and the ear-occluded coupler in order to obtain the typical flat frequency response below the resonance frequency of the system.

[10]

2. MEASUREMENT SETUP

For a better understanding of the model, the loudspeaker and the measurement setup are described first. The loudspeaker, whose geometry and manufacturing process is detailed in [4] is composed of bending piezoelectric actuators manufactured in a first Silicon On Insulator (SOI) wafer on which a rigid plate manufactured in a second SOI wafer is bonded. This rigid plate can freely move out-of-plane and the harmonic oscillation of the latter creates an acoustic pressure. A picture of one loudspeaker is depicted in Figure 1. It shows the custom made printed circuit board in green, on which the loudspeaker is glued and wire-bonded. On the picture, the grid composed of the stiffeners of the rigid plate of the loudspeaker is visible. As the loudspeaker is not integrated into a dedicated in-ear packaging it needs to be adapted in order to be used with the ear-occluded coupler. For this purpose a 3D printed adapter is designed to be bolted on the printed circuit board. In the centre of the adapter, a hollow protrusion whose dimensions are slightly larger than the moving plate is pressed against the rigid frame of the loudspeaker. The coupler is then assembled against the adapter.

Figure 2 depicts a cross section view of the complete assembly of the measurement setup. On the left, the printed circuit board with a thickness of 1.6 mm appears in green. On this printed circuit board, the loudspeaker appears in purple. On the top and the bottom of the printed circuit board, two terminal blocks are used for the electrical connection of the loudspeaker. The adapter is represented in a dark shade of grey and the duct within the adapter, between the loudspeaker and the coupler is represented in green. The duct of the adapter is then assembled with the G.R.A.S. RA0045 ear-occluded coupler, which is first composed of a conical duct usually used for the sealing plugs of earphones. The measurement setup consists in two successive ducts, a cylindrical and a conical one between the loudspeaker and the ear-occluded coupler.

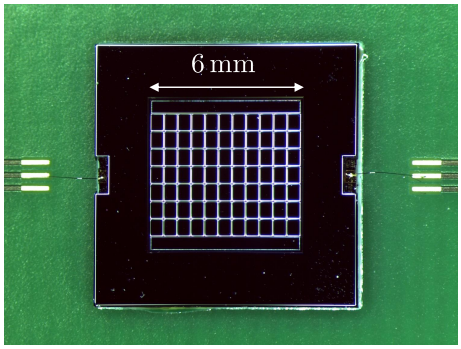

Figure 1: Photo of the loudspeaker bonded on a printed circuit board

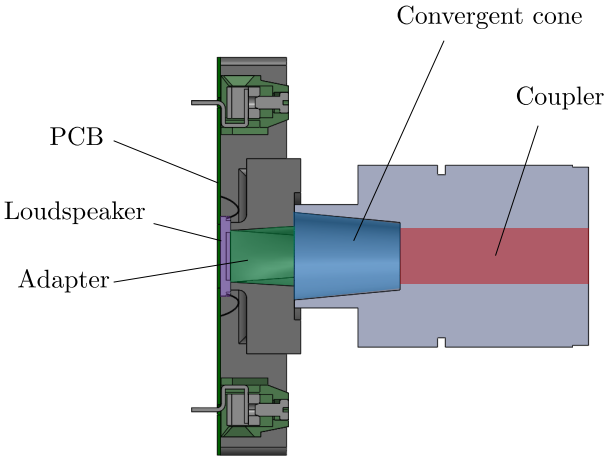

Figure 2: Cross section CAD drawing view of the loudspeaker assembly

3. LUMPED ELEMENT MODEL

The lumped element model of the loudspeaker itself is detailed more precisely in [4]. The equivalent electrical

circuit of the measurement setup consists of three different domains and is represented in Figure 3. The first equivalent circuit is the one representing the behaviour of the piezoelectric layer in low frequencies, mainly acting as a capacitor C_p as well as a resistor R_g, representing the dissipation due to the current i_{in} in pads and wires. This circuit is coupled to the mechanical one through a transformer of ratio ζ, representing the conversion of the voltage u_c across the capacitor C_p to a force F_{in} due to the piezoelectric effect, actuating a first order mechanical resonator composed of an equivalent viscous damping R_{ms}, an apparent compliance C_{ms} and an effective moving mass M_{ms}. This mechanical circuit is coupled to an acoustical circuit by a transformer of ratio S_d^{-1}, representing the effective radiating surface of the loudspeaker. In our case, the acoustical circuit is composed of two successive ducts, a cylindrical and a conical ones, representing the adapters used to adapt the moving plate of the loudspeaker to the ear-occluded coupler represented by a quadrupole on the right. The complete circuit representing the ear-occluded coupler is given in Figure 5. Parameters for the loudspeaker are taken from [4] and are recalled in Table 1.

Both the conical and the cylindrical tubes are simulated as quadrupole elements and represented analytically by transfer matrices, connecting the input volume velocity and the input pressure to the output volume velocity and output pressure such as

$$\begin{bmatrix} p_{in} \\ Q_{in} \end{bmatrix} = \begin{bmatrix} A & B \\ C & D \end{bmatrix} \begin{bmatrix} p_{out} \\ Q_{out} \end{bmatrix}. \tag{1}$$

where A, B, C and D are determined analytically and are equal to

$$\begin{cases} A_d = \cos k_c L \\ B_d = jZ_c \sin k_c L \\ C_d = \dfrac{j}{Z_c} \sin k_c L \\ D_d = \cos k_c L \end{cases} \tag{2}$$

for a cylindrical tube of length L and of characteristic impedance Z_c written

$$Z_c = \frac{\rho_0 c_0}{S} \tag{3}$$

and

$$k_c = k_0 + (1-j)\alpha \tag{4}$$

the complex wave number, taking into account visco-thermal losses on boundaries.

For a convergent conical duct, whose dimensions are represented in Figure 4, coefficients of the transfer matrix derived in [11] write

$$\begin{cases} A_c = \dfrac{R_{i+1}}{R_i} \cosh \Gamma \ell - \dfrac{\beta}{\Gamma_i} \sinh \Gamma_i \ell \\ B_c = \dfrac{R_{i+1}}{R_i} Z_{c,i} \sinh \Gamma_i \ell \\ C_c = \dfrac{1}{Z_{c,i}} \left[\left(\dfrac{R_{i+1}}{R_i} - \dfrac{\beta^2}{\Gamma_i^2} \right) \sinh \Gamma_i \ell + \dfrac{\beta^2 \ell}{\Gamma_i} \cosh \Gamma_i \ell \right] \\ D_c = \dfrac{R_i}{R_{i+1}} \left(\cosh \Gamma_i \ell + \dfrac{\beta}{\Gamma_i} \sinh \Gamma_i \ell \right) \end{cases} \tag{5}$$

where ℓ is the length of the cone and R_i and R_{i+1} are respectively the input and the output radii of the duct, $\overline{R_i}$ is the equivalent cylindrical radius written as

$$\overline{R_i} = (2 \min(R_i, R_{i+1}) + \max(R_i, R_{i+1}))/3, \tag{6}$$

and

$$\beta = \frac{R_{i+1} - R_i}{\ell R_i}. \tag{7}$$

The propagation wave number Γ_i can be expressed as

$$\Gamma_i = \frac{j\omega}{c_0} \sqrt{\frac{1 + (\gamma - 1)\mathcal{J}(k_t \overline{R_i})}{1 - \mathcal{J}(k_v \overline{R_i})}}, \tag{8}$$

with

$$k_v = \sqrt{j\omega \frac{\rho}{\mu}}. \tag{9}$$

The characteristic impedance of the cone writes

$$Z_{c,i} = \frac{\rho c_0}{\pi R_i^2} \sqrt{\frac{(1 + (\gamma - 1)\mathcal{J}(k_t \overline{R_i}))^{-1}}{1 - \mathcal{J}(k_v \overline{R_i})}}, \tag{10}$$

with

$$k_t = \sqrt{j\omega\rho \frac{c_p}{\kappa}}. \tag{11}$$

The function $\mathcal{J}(z)$ represents the dissipative terms and writes

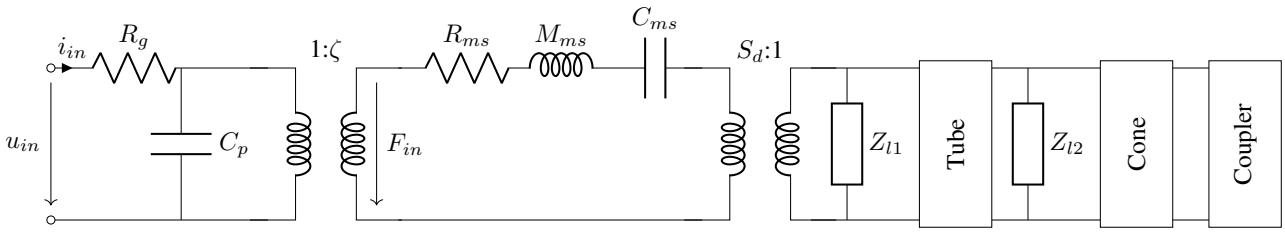

Figure 3: Equivalent electrical circuit of a piezoelectric loudspeaker radiating into two ducts and an ear-occluded coupler

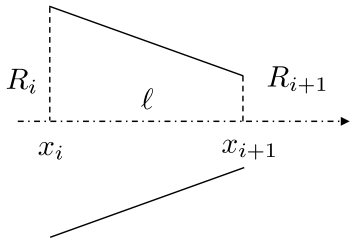

Figure 4: Definition of the geometrical quantities for a convergent cone adapted from [11]

$$\mathcal{J}(z) = \frac{2J_1(z)}{zJ_0(z)} \tag{12}$$

with J_0 and J_1 Bessel functions of the first kind and of respectively zero and first orders. Values for c_0 the sound velocity, ρ_0 the density of air, μ the viscosity of air, κ the thermal conductivity of air, c_p the specific heat with constant pressure and γ the ratio of specific heats are given in Table 1. The coupler represented as a quadrupole in Figure 3 can be simulated by an equivalent electrical circuit given in [12] and depicted in Figure 5. Between the loudspeaker and the first duct, as well as between the first duct and the second duct, leakage impedances $Z_{l,1}$ and $Z_{l,2}$ are introduced. Leakages in headphones design are often represented as a series inductor and resistor [13], such as

$$Z_{l,n} = R_{l,n} + j\omega L_{l,n}. \tag{13}$$

Once transfer matrices are derived for both ducts, the complete circuit can be expressed as a single matrix resulting of the product of all matrices such as it is derived in Equation 14.

Table 1: Lumped elements parameters of the loudspeaker

Parameter	Value	Unit
c_0	343	$\mathrm{m\,s^{-1}}$
ρ_0	1.2	$\mathrm{kg\,m^{-3}}$
μ	18.5	$\mathrm{\mu Pa\,s}$
κ	0.026	$\mathrm{W\,m^{-1}\,K^{-1}}$
γ	1.402	–
c_p	91	nF
ζ	0.49	$\mathrm{mN\,V^{-1}}$
R_{ms}	4	$\mathrm{\mu N\,s\,m^{-1}}$
M_{ms}	3.8	mg
C_{ms}	5.7	$\mathrm{mm\,N^{-1}}$
S_d	36	$\mathrm{mm^2}$
L_1	82.9	$\mathrm{Pa\,s^2\,m^{-3}}$
L_2	9400	$\mathrm{Pa\,s^2\,m^{-3}}$
L_3	130.3	$\mathrm{Pa\,s^2\,m^{-3}}$
L_4	983.8	$\mathrm{Pa\,s^2\,m^{-3}}$
L_5	133.4	$\mathrm{Pa\,s^2\,m^{-3}}$
C_1	1	$\mathrm{pPa\,m^{-3}}$
C_2	1.9	$\mathrm{pPa\,m^{-3}}$
C_3	1.5	$\mathrm{pPa\,m^{-3}}$
C_4	2.1	$\mathrm{pPa\,m^{-3}}$
C_5	1.517	$\mathrm{pPa\,m^{-3}}$
R_2	50.6	$\mathrm{MPa\,s\,m^{-3}}$
R_4	31.1	$\mathrm{MPa\,s\,m^{-3}}$

$$\begin{bmatrix} p_{in} \\ Q_{in} \end{bmatrix} = \begin{bmatrix} 1 & R_s \\ 0 & 1 \end{bmatrix} \begin{bmatrix} 1 & 0 \\ j\omega C_p & 1 \end{bmatrix} \begin{bmatrix} \frac{1}{\gamma} & 0 \\ 0 & \gamma \end{bmatrix} \begin{bmatrix} 1 & R_{ms} \\ 0 & 1 \end{bmatrix} \begin{bmatrix} 1 & j\omega M_{ms} \\ 0 & 1 \end{bmatrix} \begin{bmatrix} 1 & \frac{1}{j\omega C_{ms}} \\ 0 & 1 \end{bmatrix} \tag{14}$$
$$\begin{bmatrix} S_d & 0 \\ 0 & \frac{1}{S_d} \end{bmatrix} \begin{bmatrix} 1 & 0 \\ \frac{1}{R_{l1}+j\omega L_{l1}} & 1 \end{bmatrix} \begin{bmatrix} A_d & B_d \\ C_d & D_d \end{bmatrix} \begin{bmatrix} 1 & 0 \\ \frac{1}{R_{l2}+j\omega L_{l2}} & 1 \end{bmatrix} \begin{bmatrix} A_c & B_c \\ C_c & D_c \end{bmatrix} \begin{bmatrix} 1 & j\omega L_1 \\ 0 & 1 \end{bmatrix}$$
$$\begin{bmatrix} 1 & 0 \\ \frac{1}{j\omega C_1} & 1 \end{bmatrix} \begin{bmatrix} 1 & 0 \\ Z_2 & 1 \end{bmatrix} \begin{bmatrix} 1 & j\omega L_2 \\ 0 & 1 \end{bmatrix} \begin{bmatrix} 1 & 0 \\ \frac{1}{j\omega C_3} & 1 \end{bmatrix} \begin{bmatrix} 1 & 0 \\ Z_4 & 1 \end{bmatrix} \begin{bmatrix} 1 & j\omega L_5 \\ 0 & 1 \end{bmatrix} \begin{bmatrix} 1 & 0 \\ \frac{1}{j\omega C_5} & 1 \end{bmatrix} \begin{bmatrix} p_{out} \\ Q_{out} \end{bmatrix}.$$

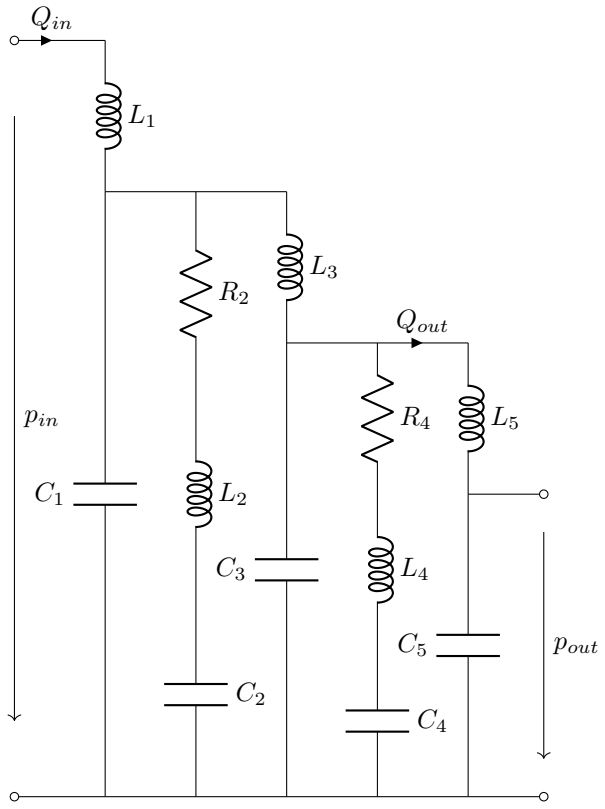

Figure 5: Lumped equivalent network of the coupler

with

$$Z_2 = R_2 + j\omega L_2 + \frac{1}{j\omega C_2} \tag{15}$$

and

$$Z_4 = R_4 + j\omega L_4 + \frac{1}{j\omega C_4}. \tag{16}$$

From Equation 14, the output pressure at the coupler microphone can be written as

$$p_{out} = \frac{Z_{out}}{\mathcal{A}Z_{out} + \mathcal{B}}. \tag{17}$$

where $\mathcal{A}$ and $\mathcal{B}$ are the coefficients of the matrix resulting of the product of all matrices.

4. RESULTS

In this section the acoustic pressure measured inside the ear-occluded coupler is compared with the one simulated using the lumped element model. As leakages are difficult to estimate, the value of resistors $R_{l,1}$ and $R_{l,2}$ and inductor $L_{l,1}$ and $L_{l,2}$ are roughly estimated using typical values and are then adjusted to fit the measurement. The influence of leakages on the frequency response is given in Figure 6. For a perfect sealing of both ducts on the loudspeaker and the coupler, corresponding to $R_{l,1} = R_{l,2} = \infty$, the frequency response is flat down to static pressure below the resonance frequency, and the resonances of the ducts and the coupler, at 5760, 11 540 and 15 540 Hz respectively are lightly damped. For a significant leakage between the loudspeaker and the cylindrical duct, with a value of $R_{l,1} = 1\,\mathrm{MPa\,s\,m^{-3}}$, the level in low frequencies is significantly decreased, of about 40 dB at 20 Hz, and the shape of the frequency response is similar to a band-pass filter. The resonance at approximately 1 kHz corresponds to the resonance of the loudspeaker in free field. In the previous case, the resonance was higher, at 1240 Hz, which corresponds to the resonance of the loudspeaker inside the closed volume. For a significant leakage between the cylindrical and the conical duct, a similar effect is observed below the resonance frequency. Above the resonance, resonances of both ducts which were bypassed by the leakage caused by $R_{l,2}$ in the previous case appear in the frequency response. They are shifted compared to

the sealed case. When both leakages are significant with $R_{l,1} = R_{l,2} = 1\,\mathrm{MPa\,s\,m^{-3}}$, the overall sound pressure level is decreased further, and resonances due to ducts are damped.

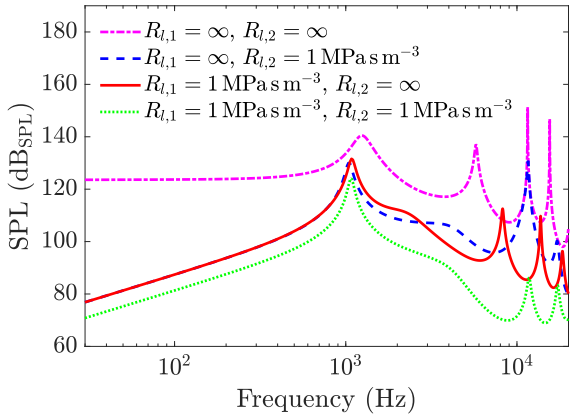

Figure 6: Pressure response simulated for different values of $R_{l,1}$ and $R_{l,2}$

The frequency response is measured using an exponential chirp signal of equation

$$x(t) = \sin\left(\phi_0 + 2\pi f_0 \left(\frac{k^t - 1}{\ln k}\right)\right) \qquad (18)$$

and of amplitude $15\,\mathrm{V_{DC}} \pm 7.5\,\mathrm{V_{DC}}$ at the output of the amplifier. The signal is amplified by a custom made DC coupled amplifier with a gain of 15 and is able to provide the DC voltage of 15 V. The microphone of the GRAS RA0045 ear-occluded coupler is externally polarized and amplified by a GRAS 12AK before being connected to the PXI-4461 module. The measurement setup is calibrated using a GRAS 42AG. Measurements are presented with a smoothing octave filter of $N = 1/12$. In Figure 7, the measured frequency response is compared with the simulated one. Below the resonance frequency, the decrease of the pressure with the decrease of the frequency due to the acoustical leakages is well estimated by choosing a value of $R_{l,1} = 80\,\mathrm{MPa\,s\,m^{-3}}$ and $R_{l,2} = 1\,\mathrm{GPa\,s\,m^{-3}}$. There is a mismatch of level of approximately 3 dB between the measured and the simulated curves below the resonance frequency. A shift of 10 % of the first resonance frequency is also observed. The second resonance, due to the impedance of the coupler and the ducts is also correctly estimated, but is highly underdamped in the model. Higher in frequency, the lumped model used for the loudspeaker as well as the plane wave assumption used for the ducts are not valid and results are diverging. At the resonance, a pressure of 140 dB$_{\mathrm{SPL}}$ was reached. In low frequency, the acoustic pressure is affected by leakages, and a pressure of 112 dB$_{\mathrm{SPL}}$ was reached. With a perfect sealing, a pressure of more than 120 dB$_{\mathrm{SPL}}$ is expected.

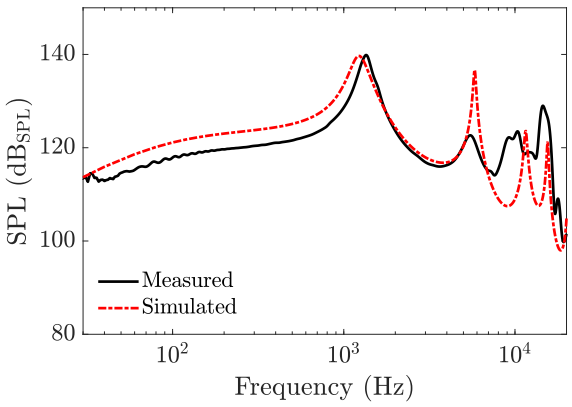

Figure 7: Pressure response simulated and measured at $u_{in} = 7.5\,\mathrm{V}$

In Figure 8, the THD of the loudspeaker is evaluated at 100 Hz for different input voltages. Below the resonance frequency, the geometrical non-linearities are maximum. For an input voltage $u_{in} = 2.4\,\mathrm{V}$ which corresponds to a sound pressure level of 100 dB$_{\mathrm{SPL}}$, a THD of 2.5 % is measured. The THD increases exponentially with the input voltage, which leads to a value of approximately 20 % for an input voltage of $u_{in} = 7.5\,\mathrm{V}$. The sound pressure level should increase linearly with the input voltage, but a non-linear effect is observed due to geometrical and acoustical non-linearities. Due to the leakage and the decrease of the sound pressure level in lower frequencies, harmonics are amplified by the transfer function and the THD is overestimated below the resonance frequency.

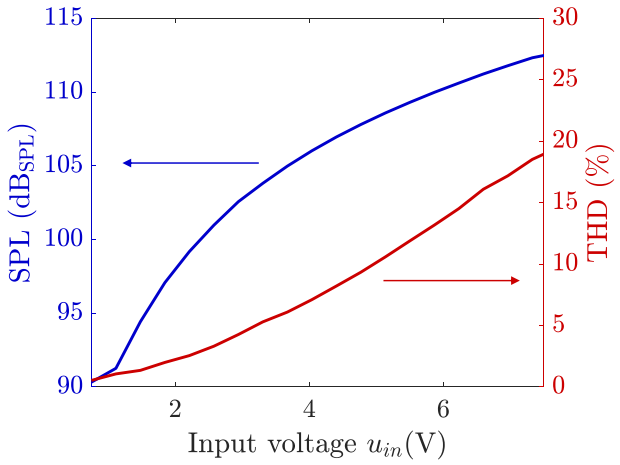

Figure 8: Sound pressure level and total harmonic distortion at 100 Hz for different input voltages u_{in}

5. CONCLUSION

In this paper, the performance of a piezoelectric MEMS loudspeaker for in-ear applications was evaluated. Due to a higher sensitivity, the loudspeaker is radiating pressures above 120 $\mathrm{dB_{SPL}}$ in a wide frequency band with a reasonably low THD. At the resonance of the loudspeaker inside the coupler a pressure of more than 140 $\mathrm{dB_{SPL}}$ was measured. With a correct sealing and a dedicated packaging, resulting in a smaller volume, sound pressure levels of more than 130 $\mathrm{dB_{SPL}}$ are expected. This loudspeaker could be successfully integrated into earphones to replace advantageously classical micro-loudspeakers.

6. ACKNOWLEDGMENTS

We would like to thank the Carnot Institute for the funding for this research.

7. REFERENCES

[1] G. Massimino, C. Gazzola, V. Zega, S. Adorno, and A. Corigliano, "Ultrasonic piezoelectric mems speakers for in-ear applications: Bubbles-like and pistons-like innovative designs," in *2022 23rd International Conference on Thermal, Mechanical and Multi-Physics Simulation and Experiments in Microelectronics and Microsystems (EuroSimE)*, pp. 1–4, IEEE, 2022.

[2] Y. Lang, C. Liu, A. Fawzy, C. Sun, S. Gong, and M. Zhang, "Piezoelectric bimorph mems speakers," *Nanotechnology and Precision Engineering*, vol. 5, no. 3, p. 033001, 2022.

[3] A. Fawzy, "Membraneless piezoelectric mems speakers based on aln thin film," *JES. Journal of Engineering Sciences*, vol. 50, no. 1, pp. 1–8, 2022.

[4] R. Liechti, S. Durand, T. Hilt, F. Casset, C. Dieppedale, T. Verdot, and M. Colin, "A piezoelectric mems loudspeaker lumped and fem models," in *2021 22nd International Conference on Thermal, Mechanical and Multi-Physics Simulation and Experiments in Microelectronics and Microsystems (EuroSimE)*, pp. 1–8, IEEE, 2021.

[5] R. Liechti, S. Durand, T. Hilt, F. Casset, C. Dieppedale, T. Verdot, and M. Colin, "A piezoelectric mems loudspeaker for in-ear and free field applications lumped and finite element models," *Microelectronics Reliability*, vol. 134, p. 114555, 2022.

[6] F. Stoppel, A. Männchen, F. Niekiel, D. Beer, T. Giese, and B. Wagner, "New integrated full-range mems speaker for in-ear applications," in *2018 IEEE Micro Electro Mechanical Systems (MEMS)*, pp. 1068–1071, IEEE, 2018.

[7] B. Kaiser, S. Langa, L. Ehrig, M. Stolz, H. Schenk, H. Conrad, H. Schenk, K. Schimmanz, and D. Schuffenhauer, "Concept and proof for an all-silicon mems micro speaker utilizing air chambers," *Microsystems & Nanoengineering*, vol. 5, no. 1, p. 43, 2019.

[8] A. Männchen, F. Stoppel, T. Brocks, F. Niekiel, D. Beer, and B. Wagner, "Design and electroacoustic analysis of a piezoelectric mems in-ear headphone," in *Audio Engineering Society Conference: 2019 AES INTERNATIONAL CONFERENCE ON HEADPHONE TECHNOLOGY*, Audio Engineering Society, 2019.

[9] S. Olive, T. Welti, and E. McMullin, "Listener preferences for different headphone target response curves," in *Audio Engineering Society Convention 134*, Audio Engineering Society, 2013.

[10] C.-H. Huang, S. Pawar, Z.-J. Hong, and J. H. Huang, "Earbud-type earphone modeling and measurement by head and torso simulator," *Applied acoustics*, vol. 73, no. 5, pp. 461–469, 2012.

[11] J. Chabassier and R. Tournemenne, *About the transfert matrix method in the context of acoustical wave*

propagation in wind instruments. PhD thesis, INRIA Bordeaux, 2019.

[12] L. Nielsen, A. Schuhmacher, B. Liu, and S. Jonsson, "Simulation of the iec 60711 occluded ear simulator," in *Audio Engineering Society Convention 116*, Audio Engineering Society, 2004.

[13] J. Borwick, *Loudspeaker and headphone handbook*. CRC Press, 2012.